Proceedings of the ASME Internal Combustion Engine Division 2007 Fall Technical Conference
ICEF2007
October 14-17, 2007, Charleston, South Carolina, USA

ICEF2007-1685

MODELING CYCLIC VARIABILITY IN SPARK-ASSISTED HCCI

C. Stuart Daw, K. Dean Edwards, Robert M. Wagner and Johney B. Green, Jr.
Fuels, Engines, and Emissions Research Center
Oak Ridge National Laboratory
2360 Cherahala Blvd, Knoxville TN 37932-6472, USA

ABSTRACT

Spark assist appears to offer considerable potential for increasing the speed and load range over which homogeneous charge compression ignition (HCCI) is possible in gasoline engines. Numerous experimental studies of the transition between conventional spark-ignited (SI) propagating-flame combustion and HCCI combustion in gasoline engines with spark assist have demonstrated a high degree of deterministic coupling between successive combustion events. Analysis of this coupling suggests that the transition between SI and HCCI can be described as a sequence of bifurcations in a low-dimensional dynamic map. In this paper we describe methods for utilizing the deterministic relationship between cycles to extract global kinetic rate parameters that can be used to discriminate multiple distinct combustion states and develop a more quantitative understanding of the SI-HCCI transition. We demonstrate the application of these methods for indolene-containing fuels and point out an apparent HCCI mode switching not previously reported. Our results have specific implications for developing dynamic combustion models and feedback control strategies that utilize spark-assist to expand the operating range of HCCI combustion.

INTRODUCTION

Homogeneous charge compression ignition (HCCI) is of considerable interest because it can significantly reduce peak in-cylinder temperatures and nitrogen oxide (NO_x) formation in internal combustion engines. In pure HCCI (that is, the ideal limit), ignition occurs as the result of compression heating of a pre-mixed fuel-air charge, and the combustion reactions occur uniformly throughout the combustion chamber with little or no flame. This is very different from conventional diesel combustion, in which fuel is injected into air that has previously been compressed and heated prior to mixing. In the latter case, combustion occurs more slowly in the form of a well-defined diffusion flame. In between pure HCCI and conventional diesel, there are intermediate forms of combustion where a portion of the fuel and air are mixed prior to combustion. These HCCI-like combustion modes are typically referred to generally as low temperature combustion modes, which are also of current interest to advanced engine researchers **[1]**.

HCCI is also very different from conventional spark-ignited combustion in which a propagating flame is initiated by an electric spark in a pre-mixed fuel-air charge **[2]**. Under some circumstances, it is possible for both HCCI and spark-ignited combustion to occur in the same cycle. One example of this dual-mode situation is illustrated in **Figure 1**, where an initial spark-ignited propagating flame compresses unburned end gases in the cylinder to the point at which HCCI is initiated in the fuel-air portion that remains unburned. Our focus in this paper is on experimental studies of a gasoline-fueled engine where scenarios such as that illustrated in **Figure 1** can occur.

In order to achieve HCCI, it is typically necessary to preheat the fuel-air mixture to within a relatively narrow temperature window prior to compression. With too low an initial temperature, HCCI will not occur. With too high an initial temperature, the HCCI burning rate can be so rapid that mechanical damage results. Preheating is often achieved through exhaust gas recirculation (EGR), and some studies have shown that the presence of certain residual gas species can also affect ignition **[3-4]**. In practice it is very difficult to achieve pure HCCI at all speeds and loads on most engines, so there is much ongoing research into how to maximize the operating envelope for HCCI **[1,5-7]**. One promising approach being considered is to switch between HCCI and spark-ignited (SI) combustion as speed and load change. Several recent publications and presentations **[8-11]** have addressed SI-HCCI switching, but with few exceptions (*e.g.*, **[12]**) there has been

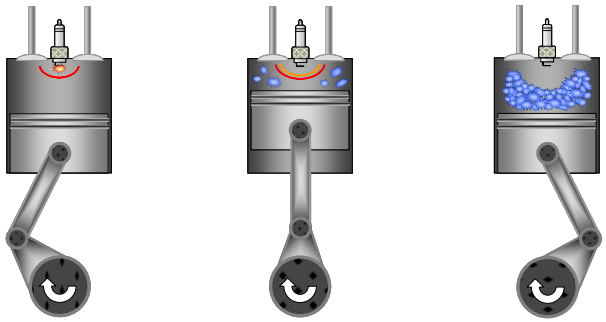

Figure 1. Illustration of the possible role of the initial SI flame in spark-assisted HCCI. The SI flame stimulates subsequent HCCI by compressing and preheating the remaining unburned gases.

limited exploration of the fundamental processes involved in transitioning between a propagating flame and HCCI.

In this paper we describe an analysis of experimental observations of unstable combustion in the SI-HCCI transition that occurs when SI is used to promote HCCI. Our goal is to understand the transition process in terms of global reaction kinetics. We are motivated to find ways of empirically observing these global kinetics directly with an engine because the results will account for in-cylinder details that would be present when trying to implement realistic on-board diagnostics and controls. We also want to correlate our phenomenological kinetics with the kinetics measured under more ideal laboratory conditions (*e.g.*, rapid compression machines) or predicted from detailed computational models. By bridging these different perspectives, we hope to improve the overall understanding and utilization of HCCI.

We base the present discussion on experimental data from a single-cylinder gasoline engine, which has been specially modified to permit internal EGR. The level of internal EGR can be precisely controlled by adjusting the timing and lift of the intake and exhaust valves, so that it is possible to vary the combustion incrementally from pure SI to pure HCCI. We find that measurements of the unstable combustion occurring at intermediate EGR levels are rich in information about the kinetics that moderate the SI-HCCI transition.

NOMENCLATURE

- $CE(i)$ = fraction of the total fuel-air charge in the cylinder in cycle i consumed by combustion (-)
- $CE_p(i)$ = fraction of the fuel-air charge left at TDC that is consumed by combustion after TDC (-)
- $CE_s(i)$ = fraction of the initial fuel-air charge consumed by combustion between the spark and TDC (-)
- COV = coefficient of variation in IMEP
- EGR = exhaust gas recirculation
- f = fraction of exhaust recirculated between cycles per unit mass fresh charge (-)
- HCCI = homogeneous charge compression ignition
- $HR(i)$ = integrated heat release in cycle i (kJ/unit mass of fresh charge)
- i = cycle index
- $IMEP$ = indicated mean effective pressure (bar)
- k_p = a global post-TDC reaction rate constant (1/s)
- $mr(i)$ = mass of residual fuel-air charge input to cycle i per unit mass of fresh charge (-)
- n = empirical parameter used in Wiebe-like combustion expression (-)
- Q = heat released/unit mass of fuel-air charge burned (kJ/mass)
- SI = spark ignition
- S_L/S_{L0} = ratio of laminar flame speed with dilution to undiluted flame speed (-)
- t_b = post-TDC burn time (s)
- TDC= top-dead-center point of engine cycle
- x_b = charge dilution fraction at spark (-)

EXPERIMENTAL

Our experimental observations were made using a 0.5-L single-cylinder AVL research engine with 11.34:1 compression ratio. This engine has two intake valves and one exhaust valve and is equipped with a full-authority hydraulic variable valve actuation (VVA) system. Internal EGR is achieved using negative valve overlap. Only a single intake valve was used in this study to promote swirl and mixing. The fuel (indolene and indolene-ethanol mixtures) was delivered by an intake mounted port fuel injector. Engine speed was maintained constant using an absorbing/motoring dynamometer. Nominal operating conditions corresponded to 1600 rpm and 3.4 bar indicated mean effective pressure (IMEP). Throughout the EGR range, spark timing was held fixed at 25°BTDC and coolant temperature maintained at 90°C. At EGR levels typically in excess of 55%, full HCCI operation was achieved, and the spark could be turned off with no impact on combustion. Fueling rate was maintained constant, and intake throttling used to maintain a stoichiometric air-fuel ratio. Typically, the throttle was wide open for pure HCCI operation.

In-cylinder pressure measurements were recorded at 0.5 crank-angle-degree of resolution for each internal EGR level. To minimize non-combustion artifacts, all engine feedback controllers were shut off, and the engine was operated in open-loop mode except for the dynamometer speed controller and coolant temperature controller. Measurements at each specific EGR level typically included 2800 consecutive engine cycles.

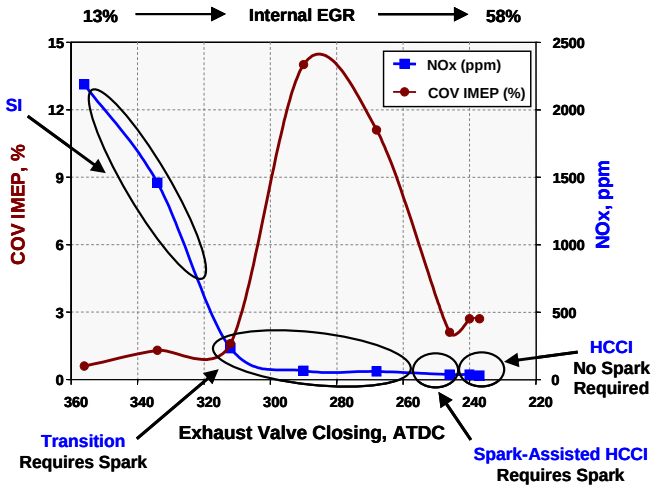

Figure 2. General combustion trends observed in the SI-HCCI transition experiments.

Standard exhaust gas instrumentation was used to provide a basic knowledge of the exhaust chemistry including steady-state measurements of CO, CO_2, HC, NO_x, and O_2 concentrations in the raw engine-out exhaust. The normal procedure following each incremental EGR adjustment was to allow the engine to run several minutes to reach 'steady-state' (for oscillatory combustion states, this meant that the behavior became statistically stationary or consistent over time). Following this runout period, in-cylinder pressure and standard engine temperature and exhaust gas analyses were recorded for the required time. Cycle resolved heat release rate, integrated heat release (HR), and indicated mean effective pressure (IMEP) were calculated from the measured in-cylinder pressure measurements following standard procedures in the literature **[2]**.

We note here that explicit measurements of the intake air-fuel ratio or in-cylinder charge stratification were not made in these experiments. As described in the next section however, the steady-state cycle-to-cycle combustion consistency for pure SI (0 EGR) and HCCI (maximum EGR) implies that the intake charge was relatively well-mixed.

RESULTS AND DISCUSSION

The global trends observed for our SI-HCCI experiments are depicted in **Figure 2**. These specific results are for indolene fueling, but similar trends were seen for indolene-ethanol fueling also. As internal EGR increased (moving from left to right), combustion shifted from pure SI combustion (with a very low COV) to a complex mixture of SI and HCCI and finally to pure HCCI (again with a low COV) when the EGR level reached about 60%. As seen in **Figure 3**, average heat release rate profiles at 0 and maximum EGR reflect the expected burn trajectories for pure SI and HCCI combustion,

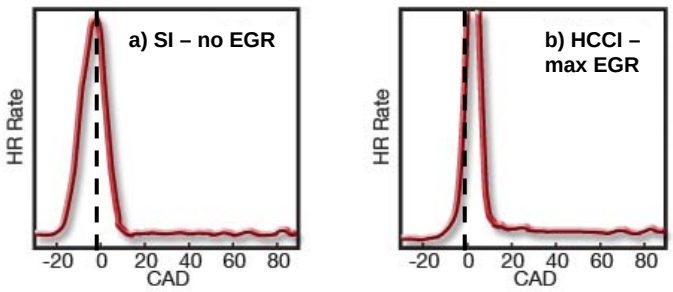

Figure 3. Heat release profiles for the limiting cases of (a) no EGR (SI) and (b) maximum EGR (HCCI)

respectively. SI heat release typically begins very soon after spark and is almost complete by TDC, while HCCI heat release rises very rapidly near TDC and occurs over a much shorter interval.

Relatively early in the transition with EGR, average NO_x emissions drop rapidly, but there was also a concomitant rise in cyclic combustion variability (indicated by the large coefficient of variation, COV, for IMEP). High COV is highly undesirable because of the erratic power delivery and unacceptable vibration that would be experienced by the driver. In addition, the occasional misfires and excessively strong combustion events that create high COV result in momentary spikes in hydrocarbon and NOx emissions, respectively (even though overall average emissions may be relatively low). Thus there is a strong incentive to introduce some type of control to smooth the transition in a way that avoids such high COV.

Our subsequent discussion focuses on the analysis of sequential cyclic combustion measurements from an intermediate EGR condition (approximately 46%). The combustion state of the engine at this EGR corresponds roughly to the point of maximum COV in IMEP (approaching 15%) in **Figure 2**. We now consider a cycle-resolved sequence of measured integrated heat release values for the target engine condition determined using the usual procedures for interpreting cylinder pressure measurements **[2]**. We correct the computed heat release values to account for cylinder-wall heat losses estimated using WAVE^{TM} engine simulation software **[13]**. For successive cycles (designated by indices *i–1* and *i*), plots such as **Figures 4(a)** and **(b)** (also referred to as first return maps) reveal the strong correlation between successive heat release values **[14-16]**. Note that the large-scale cycle-to-cycle correlation features appear similar for both pure indolene fueling (**4(a)**) and fueling with an 85/15 ethanol-indolene blend (**4(b)**).

To better understand the reasons for the observed cycle-to-cycle heat release correlations, it is helpful to consider the overall mass balance. For the fuel-air charge (assuming a stoichiometric inlet mixture) such a balance requires that

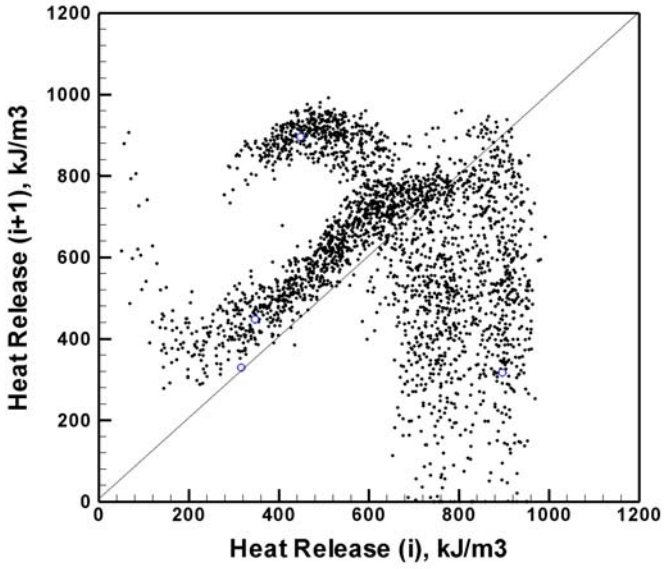

(a) Indolene

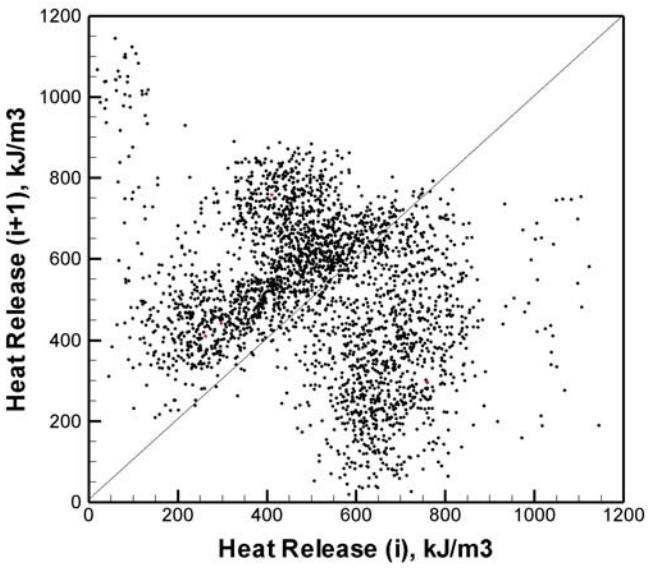

(b) E85 (85% ethanol, 15% indolene)

Figure 4. First return maps of cyclic heat release for (a) pure indolene and (b) E85 (85% ethanol, 15% indolene) at conditions near the maximum COV in heat release.

$$mr(i) = \frac{f}{1+f}\left(1 + mr(i-1) - \frac{HR(i-1)}{Q}\right). \qquad (1)$$

Equation 1 simply states that the amount of residual stoichiometric fuel-air mixture recycled from the current to the next cycle is determined by the total initial air-fuel charge in the previous cycle (made up of fresh and previous residual charges), the amount of burning in the previous cycle and the level of EGR (assuming uniform mixing of the cylinder contents). Thus if we know *mr(i–1)* and *HR(i–1)*, it is possible to calculate the residual fuel-air charge *mr(i)*. This process can be repeated *ad infinitum* as long as additional sequential heat release measurements are available.

A practical problem in using Eq. (1) to compute residual charges from heat release measurements is that the starting residual fraction, *mr(i–1)*, is not known *a priori*. This turns out not to be an insurmountable obstacle, however, because all subsequent iterates beyond the first are based solely on measured HR values. No matter what initial *mr* value is assumed, the resulting estimated series converges after a few cycles to the same values, as shown in **Figure 5**. By discarding a few of the initial cycle estimates, the remaining estimated residual charge series is unique.

Figure 6 illustrates the resulting cyclic patterns in the estimated residual charge values estimated as described above for the nominal EGR condition. Here we observe three distinct correlation trends between successive residual charges, implying three characteristically different types of combustion. For initial residual charges below 0.1, combustion throughout the cycle appears to be dominated by flame propagation from the spark (*i.e.*, HCCI does not appear to happen). For initial residual charges >0.1, the data are clustered into two distinct families, which are traced with red and green lines in the plot. As discussed below, these patterns appear to indicate that there are two distinct ways in which HCCI can occur after the initial pre-TDC SI burn.

A cycle-by-cycle heat balance similar to Eq. (1) above can also be used to estimate variations in residual gas temperature. Our

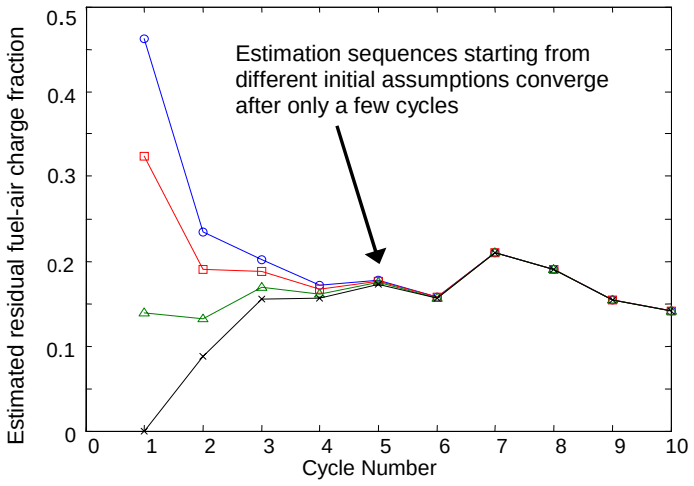

Figure 5. Convergence of iterated residual fuel-air balances for a wide range of assumed initial residual charges. Convergence is driven by repeated input from observed values of *HR(i)*.

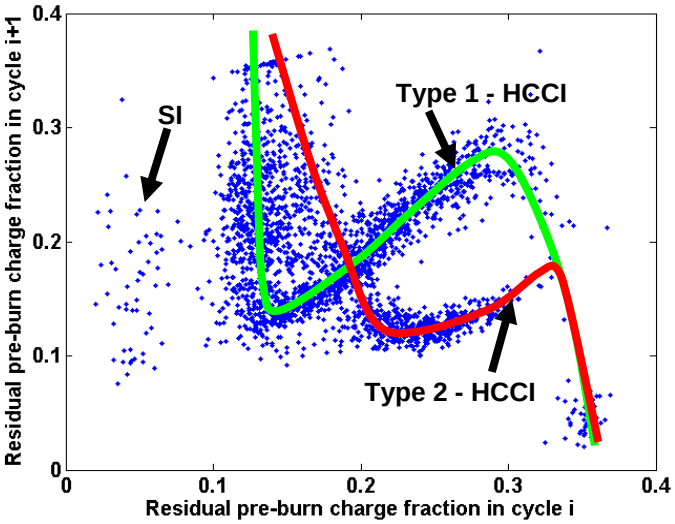

Figure 6. Characteristic patterns seen in the residual charge based on cycle-by-cycle mass balances.

detailed analysis of residual gas temperatures using appropriate heat loss estimates obtained from a WAVE engine model of our engine during both the exhaust and intake strokes convinces us that variations in exhaust temperature tend to be slower and have less immediate impact (on a cycle-to-cycle basis) compared to the variations in residual fuel-air charge. Instead, exhaust temperature variations appear to be 'filtered' by the thermal inertia of the combustion chamber and require multiple cycles over which to make substantial changes (*e.g.*, when the nominal EGR level is changed).

The relatively large cyclic impact of residual charge on subsequent combustion becomes clearer when we consider how unburned charge preheating is affected by post-spark combustion. As illustrated in **Figure 1**, post-spark flame combustion is critical to the onset of HCCI when EGR is insufficient to sustain HCCI-only combustion. In effect, the expanding flame front acts as an additional source of compression, which further boosts the preheating of the unburned gases to the point that they can ignite in the HCCI mode. Thus the effective amount of compressive boost produced depends very much on the post-spark flame speed, which is known to be highly dependent on charge dilution.

To develop quantitative estimates of the flame speed for our experiments, we estimated the nominal combustion rate for our engine under pure SI operation (no EGR) and then adjusted that rate for charge dilution with a standard flame speed correlation
[2]:

$$\frac{S_L}{S_{LO}} = 1 - 2.06 x_b^{0.77} \qquad (2)$$

where

$$x_b = 1 - \frac{1+mr}{1+f}. \qquad (3)$$

We then used a simple two-zone combustion model to estimate the unburned gas temperature at TDC in our engine at the reference nominal condition as a function of residual charge. For the subject engine condition, these estimates indicated that the unburned gas temperature at TDC can be as much as 140 K higher as the result of residual fuel-air charge coming from previous cycles.

To quantify combustion rate in each cycle we employed the concept of a global combustion efficiency, *CE(i)*. The idea behind *CE(i)* is to quantify the fraction of the fuel-air charge consumed in each cycle, analogous to the idea of fractional conversion used widely for chemical reactors. Values of *CE(i)* for our experiments were determined from the estimated heat release values and the relationship between heat release and charge depletion

$$CE(i) = \frac{HR(i)}{(1+mr(i))Q}. \qquad (4)$$

From the flame speed estimate and two-zone model described earlier, we estimated the fraction of combustion occurring as the result of spark ignition before TDC. The post-TDC contribution to combustion is then related to overall and pre-TDC combustion by

$$CE_p(i) = \frac{(CE(i) - CE_s(i))}{(1 - CE_s(i))}. \qquad (5)$$

where $CE_s(i)$ and $CE_p(i)$ are the pre- and post-TDC combustion efficiencies for cycle *i*.

To relate the post-TDC fractional conversion to a global kinetic rate, we conjectured that it is possible to use a simplified global Wiebe-type relationship:

$$CE_p(i) = 1 - e^{(-k_p t_b)^n} \qquad (6)$$

where k_p is a global reaction rate constant, t_b is a burn time, and n is an empirical exponent.

Note that taking the derivative of Eq. (6) with respect to time yields an expression that is proportional to in-cylinder heat release rate. Comparisons with our experimental heat release rate measurements indicate that this type of function does indeed provide a good fit using appropriate values for the three parameters.

Focusing on post-TDC combustion seems reasonable if we assume that the onset of HCCI tends to disrupt continuing flame propagation and that HCCI, when it occurs in the

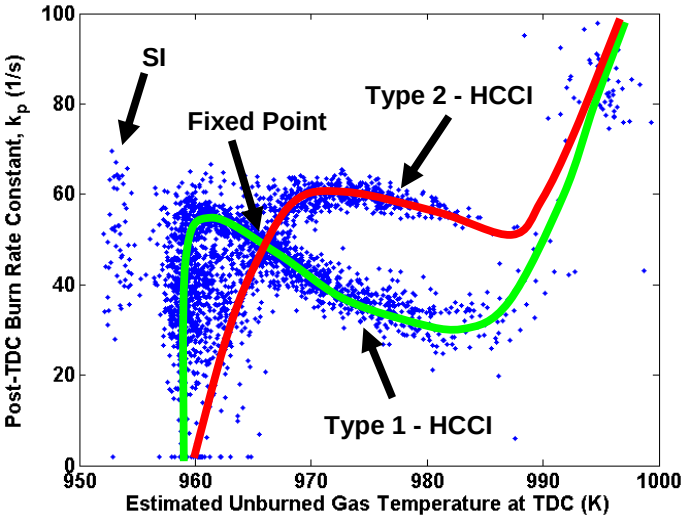

Figure 7. Relationship between the estimated global post-TDC burn rate constant and unburned gas temperature at TDC.

transition region, probably tends to initiate at or near TDC when the compression heating of the unburned gas is near maximum. Assuming that the post-TDC burn time is constant and the same for all cycles and fixed by the valve timings and engine speed, we can estimate a global post-TDC burn rate constant (k_p), which applies specifically to only that part of the combustion. We also assume that the empirical exponent is constant from cycle to cycle as well (as is typically the case for the analogous Wiebe parameter). Combining our estimates of k_p and temperature at TDC, we obtain plots such as **Figure 7**.

We expect that the global post-TDC burn rate constant should be a strong function of temperature, but obviously the trend in **Figure 7** is more complex than a simple Arrhenius relationship. Actually, there again appear to be three distinct trends (labeled in the figure) associated with the three different residuals patterns noted earlier. In analyzing the post-TDC heat release profiles for combustion events in these different regions, we see what appears to be an almost purely propagating flame (SI) combustion occurring at low temperatures and two types of HCCI (or HCCI-like) combustion occurring at higher temperatures. Both types of HCCI combustion exhibit regions of negative temperature coefficient (NTC) behavior (*i.e.*, the burn rate constant decreases with increasing temperature), but NTC is much more pronounced in one case than the other.

At one TDC temperature, the global kinetic rates of the two types of HCCI appear to cross (*i.e.*, have the same value). We know from other analyses not presented here **[14-16]** that this particular point represents an unstable fixed point of the engine dynamical system. It represents the condition when the engine is most likely to shift from one type of HCCI to the other. This is an important point to recognize because it would be a natural point at which to implement controls.

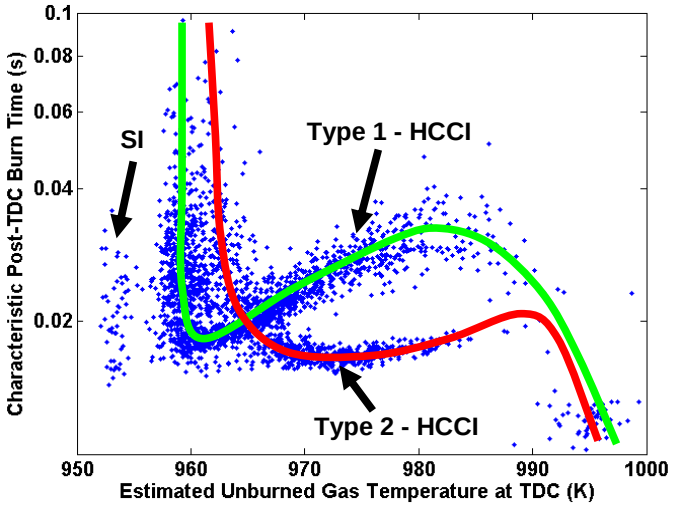

(a) Spark-assisted HCCI.
ϕ = 1.0, EGR = 46%

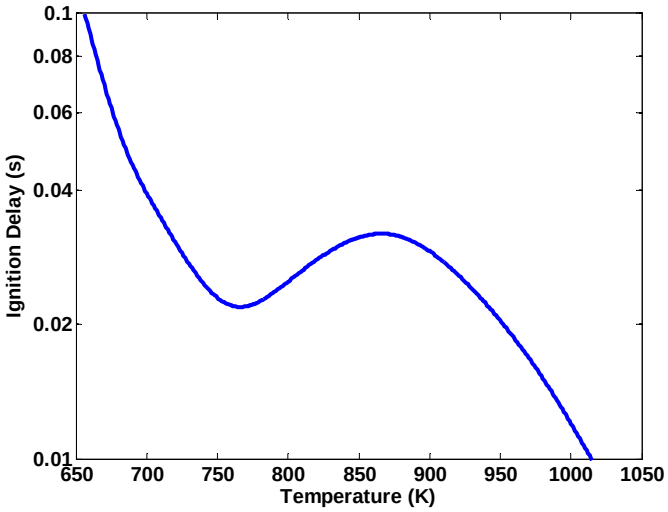

(b) Ignition delay for n-heptane from Pitsch mechanism.
ϕ = 0.4, P = 8.2 atm, Inert/O_2 = 5

Figure 8. Comparison of (a) observed post-TDC burn time ($1/k_p$) with (b) computed ignition delay for n-heptane.

For comparison with detailed kinetics models and other laboratory measurements of NTC behavior (*e.g.*, using rapid compression machines), it is useful to consider the reciprocal of k_p, which represents a global time scale for post-TDC combustion. **Figure 8(a)** illustrates the result for the same data plotted in **Figure 7**. Here curves have been added to help distinguish the trends for the two different HCCI-like patterns. Note the similarity between the type 1 HCCI trend in **Figure 8(a)** and **Figure 8(b)**, which is a plot of ignition delay for n-heptane undergoing HCCI predicted by the Pitsch mechanism **[17-18]**.

The strong similarity between the type 1 HCCI and **Figure 8(b)** suggests that at least part of the cycle-to-cycle combustion variations for our engine in the SI-HCCI transition involved n-heptane-like kinetics. Interestingly, the level of NTC behavior observed in these experiments has not been reported for indolene in other studies (as far as we have been able to determine). Although indolene is actually a complex mixture of alkanes and aromatics, it has been suggested that its behavior can be approximated by a mixture of surrogate fuels, n-heptane, iso-octane, and toluene **[19]**. This suggests to us that at least on some occasions, the appearance of n-heptane-like kinetics that characteristically have a strong NTC behavior should not be surprising for indolene.

What is perhaps more intriguing is the fact that in our engine there was a second type of HCCI for which the NTC behavior was much less pronounced but still present to a degree. This probably represents the effect of alternative kinetic pathways associated with the non-heptane-like components in indolene. The fact that the transitions between these different HCCI modes appears to occur predictably **[14-16]** indicates that there is probably a deterministic shifting of the residual composition between high and low heptane-like fractions..

To clarify, we conjecture that the heptane-like components are consumed in disproportionate amounts in some cycles, leading to one or more subsequent cycles where the non-heptane-like components dominate the chemistry and the HCCI reactions are exceptionally strong. Once the strong reactions consume the non-heptane residuals, the in-cylinder mixture returns to the higher n-heptane-like fraction present in the raw fuel. If such a residual composition shift is responsible for the kind of mode switching seen here, it might be exploited for purposes of control. For example, selected components might be deliberately added to the fresh fuel to steer the combustion away from or toward one or the other of the alternative HCCI combustion modes.

Finally, the strong similarity between the dynamical trends seen for both indolene and indolene-ethanol fuel mixtures suggests that the basic kinetic pathways for HCCI are not appreciably changed by the presence of up to 85% ethanol. This observation and those above should provide useful benchmarks for evaluating and improving the predictions of detailed in-cylinder HCCI kinetics models. Ultimately, the most useful kinetic models for HCCI will need to produce the kind of cycle-to-cycle trends reported here. In addition, the robustness of these trends in our experiments suggests that development of simplified in-cylinder combustion models based on global kinetic parameters should be possible and may be useful for correlating measurements and developing real-time diagnostics and controls.

CONCLUSIONS

Our results indicate that global kinetic parameters can be extracted from sequential unstable cycle-resolved combustion measurements in the SI-HCCI transition. For our experiments, enhancement of the pre-TDC compression heating by spark-initiated burning of the residual fuel-air charge had major impact on post-TDC combustion. When pre-TDC heating was less than a critical level, post-TDC combustion was dominated by a continuation of the initial SI burning. Above a critical level of preheating, two distinct types of HCCI combustion occurred after TDC, one exhibiting strong NTC and one weak NTC. Switching between the two HCCI modes occurred based on recent combustion history in previous cycles. The level of NTC behavior observed for indolene in these experiments has not been reported for indolene in other studies. This same general behavior appears to occur even when indolene is diluted with up to 85% ethanol.

ACKNOWLEDGMENTS

This work was sponsored by the U.S. Department of Energy, Office of Freedom Car and Vehicle Technologies. Program Managers are Steve Goguen and Gurpreet Singh. As work for the U.S. Government, this paper cannot be copyrighted.

REFERENCES

[1] DN Assanis, PM Najt, JE Dec, JA Eng, TN Asmus, F Zhao (2003). *Homogeneous Charge Compression Ignition (HCCI) Engines: Key Research and Development Issues*. SAE International. ISBN 978-0-7680-1123-4.

[2] JB Heywood (1988). *Internal Combustion Engine Fundamentals*, McGraw-Hill. ISBN 007028637X.

[3] GM Shaver, JC Gerdes, P Jain, PA Caton , CF Edwards (2003). "Modeling for Control of HCCI Engines", *Proceedings of the American Control Conference*. 749-754.

[4] PA Caton, AJ Simon, JC Gerdes, CF Edwards (2003). "Residual-effected homogeneous charge compression ignition at low compression ratio using exhaust reinduction", *International Journal of Engine Research*, 4(2).

[5] T Urushihara, K Hiraya, A Kakuhou, T Itoh (2003). "Expansion of HCCI operating region by the combination of direct fuel injection, negative valve overlap and internal fuel reformation", SAE 2003-01-0749.

[6] J Olsson, P Tunestal, B Johansson (2004). "Boosting for high load HCCI", SAE 2004-01-0940.

[7] K Duffy, A Kieser, E Fluga, D Milam (2004). "Heavy-duty HCCI Development Activities", 2004 Diesel Engine Emissions Reduction (DEER) Conference. www1.eere.energy.gov/vehiclesandfuels/pdfs/deer_2004/session7/2004_deer_duffy.pdf

[8] M Weinrotter (2005). "Optical diagnostics of laser-induced and spark plug-assisted HCCI combustion", SAE 2005-01-0129.

[9] T Urushihara, K Yamaguchi, K Yoshizawa, T Itoh (2005). "A study of gasoline-fueled compression ignition engine –

expansion of HCCI operation range using SI combustion as a trigger of compression ignition", SAE 2005-01-0180.
[10] H Santose, J Mathews, W Cheng (2005). "Managing SI/HCCI dual-mode engine operation", SAE 2005-01-0162.
[11] J Hyvonen, B Johansson (2005). "Operating conditions using spark assisted HCCI combustion during combustion mode transfer to SI in a multi-cylinder VCR-HCCI engine", SAE 2005-01-0109.
[12] L Koopmans, O Backlund, I Denbratt (2002). "Cycle to cycle variations: their influence on cycle resolved gas temperature and unburned hydrocarbons from a camless gasoline compression ignition engine", SAE 2002-01-0110.
[13] WAVE, Version 7.2 Build 16, www.ricardo.com/software.
[14] RM Wagner, KD Edwards, CS Daw, JB Green, Jr. BG Bunting (2006). "On the Nature of Cycle Dispersion in Spark-assisted HCCI Combustion", SAE 2006-01-0418.
[15] KD Edwards, CS Daw, RM Wagner, JB Green, Jr. (2006). "Cyclic Variability During the Transition Between Spark-ignited Combustion and HCCI", *Proceedings of the 2006 Technical Meeting of the Central States Section of The Combustion Institute*, 21-23 May 2006; Cleveland, OH, USA.
[16] CS Daw, RM Wagner, KD Edwards, JB Green, Jr. (2007). "Understanding the Transition Between Conventional Spark-ignited Combustion and HCCI in a Gasoline Engine", *Proceedings of The Combustion Institute*, 31.
[17] MS Wooldridge, SM Walton, X He, BT Zigler (2006). "Chemical Kinetics of Homogeneous Charge Compression Ignition and Other Low-Temperature Combustion Strategies", *Proceedings of the 2006 Technical Meeting of the Central States Section of the Combustion Institute*.
[18] S Liu, J Hewson, JH Chen, H Pitsch (2004). "Effects of Strain Rate on High-Pressure Nonpremixed n-heptane Autoignition in Counterflow", *Combustion and Flame*, 137(3), 320-339.
[19] R Ogink, VI Golovitchev (2003). "Reaction Mechanisms for Natural Gas and Gasoline in Homogeneous Charge Compression Ignition (HCCI) Engine Modeling". SAE 6th International Conference on Engines for Automobiles. ICE2003. Naples, Italy; September 2003.